Sensors & Transducers, Vol. 237, Issue 9-10, September-October 2019, pp. 67-74

www.sensorsportal.com

Sensors & Transducers

Published by IFSA Publishing, S. L., 2019
http://www.sensorsportal.com

Optimized Integrated PIN Photodiodes with Improved Backend Layers

[*] Ingrid JONAK-AUER, Frederic ROGER and Olesia SYNOOKA
ams AG, Device R&D, Tobelbaderstrasse 30, 8141 Premstaetten, Austria
[*] Tel.: +43-3136-500-32000, fax: +43-3136-500-932000
[*] E-mail: ingrid.jonak-auer@ams.com

Received: 30 August 2019 /Accepted: 27 September 2019 /Published: 30 November 2019

Abstract: This paper constitutes a systematic analysis of the impact of low-doped intrinsic base material, different bottom anti-reflective coatings and dielectric filter deposition on the electrical and optical performance of Si photodiodes processed in standard CMOS fabrication processes. Photodiode designs cover full area as well as interdigitated variants. Optimization of the photodiode's spectral responsivity for a specific wavelength has been achieved by different bottom anti-reflective coating concepts as well as direct deposition of interference filters on Si-wafer. While standard bottom anti-reflective coating is the most efficient way of optimizing the optical response, embedded bottom anti-reflective coating offers the possibility of additional interference filter deposition directly on the wafer. For full area photodiodes with respective anti-reflective coating in place, the photodiode's quantum efficiency approaches 100 % for λ=750 nm. For interdigitated photodiodes, the spectral responsivity in the wavelength range of 400 nm to 500 nm can be significantly enhanced compared to full area photodiodes and show values as high as 0.21 A/W @ 400 nm and 0.37 A/W @ 500 nm. Optimized blue photodiodes are not sensible to iEPI thicknesses and have a leakage current of 10 pA for a 150 µm×150 µm square photodiode.

Keywords: Integrated PIN Photodiode, Intrinsic epitaxial Si substrate, Bottom antireflective coating, Dielectric Filter, Spectral responsivity, Leakage current.

1. Introduction

A photodiode (PD) is a device based on a p-n junction collecting photocurrent generated in the substrate. The combination of reverse biasing and large depletion area are necessary for improving the quantum efficiency of the photodiode [1]. The depletion area can be enlarged by using low-doped intrinsic Si, thus forming a p-intrinsic-n (PIN) photodiode. The low-doped intrinsic epitaxial material (iEPI) additionally reduces the recombination rate of the photo carriers, thus improving the efficiency of the device. The ability to detect only a defined portion ("band") of incoming light with respect to wavelength is key for applications such as color sensing, spectral imaging, UV light detection and ambient light sensing. The photodiode can be tuned to be especially sensitive to specific wavelengths by using appropriate p-n junctions as well as adding a variety of add-on filters and coatings like bottom anti reflective coating (BARC), embedded bottom anti reflective coating (eBARC) and/or dielectric filters as part of the CMOS fabrication process, In this paper the impact of the different intrinsic p-type base materials, different photodiode and guard ring designs and different add-on layers are analyzed with respect to optical and electrical performance of the optical sensors.

2. Materials and Methods

For this study we designed full area photodiodes as well as interdigitated photodiodes [2]. For full area photodiodes we designed circular and square high doped shallow n-type layers in p-type iEPI (Fig. 1(a)), hereafter called nPD, For the interdigitated photodiodes we designed high doped shallow n-type and p-type fingers constituting intermeshing comb structures as depicted in Fig. 1(b). Another type of full area photodiode optimized for the blue wavelength regime is shown in Fig. 1(c). It uses a deep n-well with a counter-doped shallow p-well, thus making the photodiode less sensible to red and near infrared wavelengths. This type of photodiode will hereafter be called bluePD. By shortening deep n-well and substrate, the photocurrent generated in the iEPI recombines and does not contribute to the photocurrent collected by the bluePD.

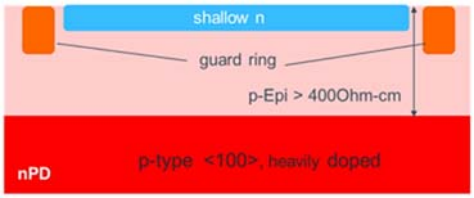

(a)

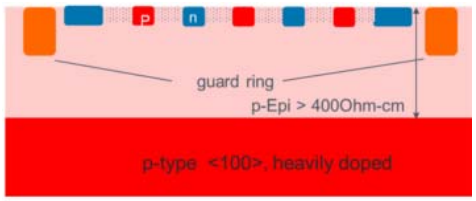

(b)

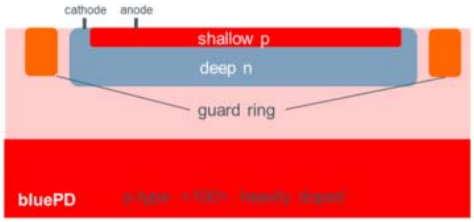

(c)

Fig. 1. PIN photodiode schematics of (a) full area nPD and (b) interdigitated PDs of alternate n-type and p-type stripes and (**c**) p-type well inserted in a deep n-type well electrically connected to substrate (bluePD).

Regarding guard ring design we have processed and analyzed photodiodes with pnp guard rings as well as photodiodes with just p-type substrate contacts of different depths.

Low doped p-type Epi of resistivity > 400 Ohm-cm on top of a highly p-doped substrate was used as base material. The advantage of an appropriately thick intrinsic EPI layer on top of a highly doped substrate is the fact that only electron hole pairs created within the space charge region of the diode contribute to the photocurrent whereas carriers generated below the space charge region recombine in the highly doped substrate

All photodiodes have been processed in an industry standard 350 nm high-voltage CMOS technology, using a very cost effective way to integrate PIN photo detectors [3]. Processing of an additional isolation well as host for all circuitry components guarantees full functionality of the standard CMOS logic while the photo detectors highly benefit from the low doping concentrations of the intrinsic material. A schematic layout of the presented PIN photodiode integration concept is shown in Fig. 2. Special surface protection techniques are performed to maintain the low doping concentrations of the substrate during the complete CMOS processing. Complete modularity of the CMOS process remains uncompromised by the implementation of PIN photodiodes.

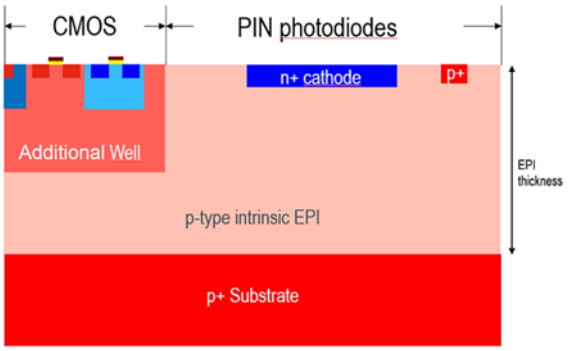

Fig. 2. Schematic layout of PIN photodiode integration concept.

The spectral responsivity of a photodiode depends largely on the efficiencies of light transmission of all layers on top of the semiconductor surface as well as the electron-hole pair generation and carrier collection. Designing a near-zero reflection antireflective coating and engineering the photodiode such that the depletion region covers the area of optimal light absorption will yield the highest responsivities. To further enhance the photo sensor's quantum efficiency in specified wavelength regimes, different anti-reflective coating concepts were applied. In the standard BARC concept [4], shown in Fig. 3(a), the reflected fraction of the optical power is minimized by removing the whole dielectric stack on top of the photodiode before BARC deposition.

For photo sensors, which require additional filter deposition or 3D integration by through silicon vias the standard BARC concept is not applicable, because 3D integration as well as filters require planar wafer surfaces for further processing. To make the general concept of an appropriate λ/4 plate also accessible to these sensors, an embedded BARC (eBARC) concept has been developed, which is shown in Fig. 3 (b).

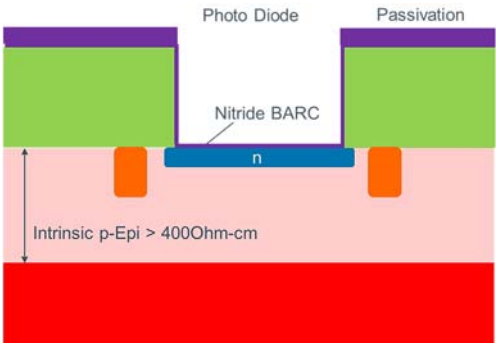

Fig. 3(a). Schematics of standard BARC concept.

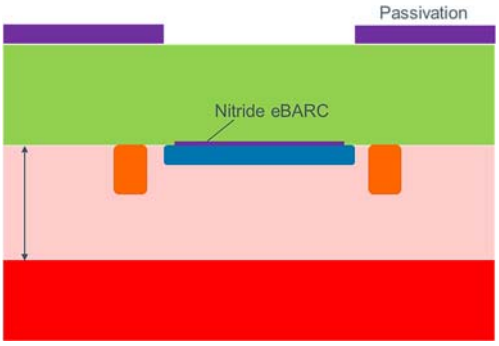

Fig. 3(b). Schematics of embedded BARC concept.

Some photodiodes were processed with dielectric filter stacks in addition to eBARC. Interference filter processing uses reactive magnetron sputtering and lift-off patterning, which permits lateral filter dimensions smaller than 100 µm. Band pass filters were designed for transmission of different spectral regimes and processed in-line with the photodiodes. Special care was taken by layout rules and wafer edge treatment to minimize mechanical stress and wafer bow for combinations of up to 6 and more filters integrated on the wafer.

Characterization of the PIN photodiodes covers capacitance and leakage current measurements as well as spectral responsivity measurements. Photodiode layout permits direct pad access to anode and cathode without any signal amplification circuit. Capacitance measurements have been performed with a Cascade Micromanipulator and a HP4284A precision LCR meter, for leakage current measurements we used the Cascade Micromanipulator equipped with thermo-chuck and a Parameter Analyzer HP4155B. All optical measurements were performed on wafer level according to the measurement setup depicted in Fig. 4. A Xenon lamp is used as light source, which is discrete band filtered in 1 nm wavelength steps via a spectrometer. The monochromatic light beam is split, one half goes into a reference detector for actual power measurement, while the other half is fed onto the optically active area of the device under test. To determine the responsivity of the device under test, the photocurrent generated by the incident light power is measured with a Parameter Analyzer HP4155B. The biasing of the photodetector device under test is also done by the Parameter Analyzer. Measurement data recordings as well as filter steering, calibration and reference light power measurements are controlled via serial bus interfaces and personal computers.

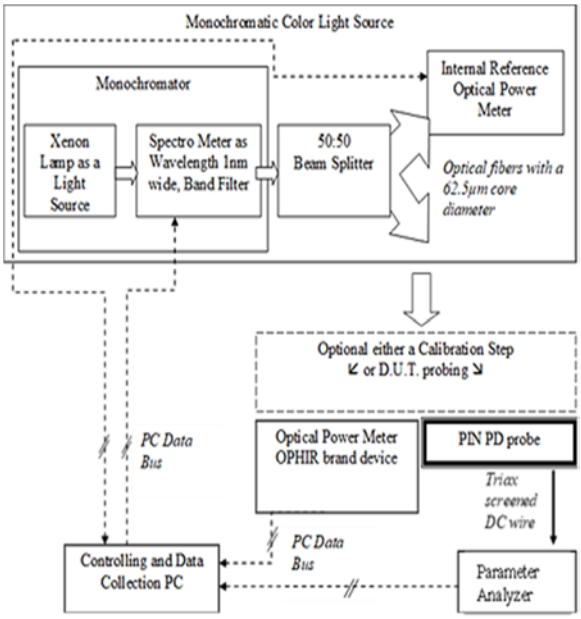

Fig. 4. Experimental setup for spectral responsivity measurements.

3. Results

Fig. 5 presents the impact of the iEPI- and BARC-thickness on spectral responsivity (SR). The spectral responsivity reaches 100 % of the quantum efficiency for BARC layers optimized for λ=750 nm and λ=900 nm and 82 % for layer optimized for λ=425 nm wavelengths.

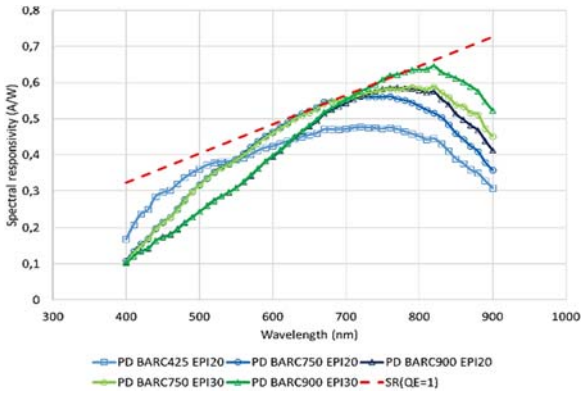

Fig. 5. Dependence of spectral responsivity on iEPI- and BARC-thickness.

The leakage current of a circular nPD of 365 µm diameter in dependence on iEPI- and BARC-thickness is shown in Fig. 6.

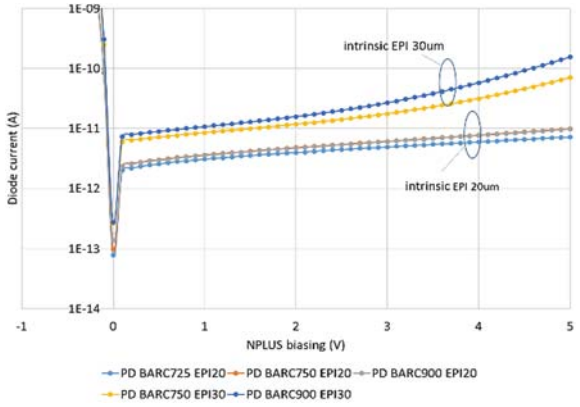

Fig. 6. Leakage current dependence on iEPI- and BARC thickness.

From a theoretical point of view, thicker iEPI should cause larger space charge width and thus higher leakage current. But TCAD simulations showed no such effect as depicted in Fig. 7, where the leakage current of nPDs has been simulated for 20 µm and 30 µm iEPI.

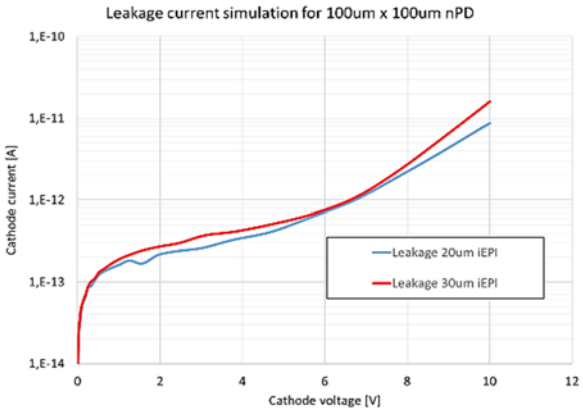

Fig. 7. TCAD simulation of nPD leakage current for two EPI thicknesses.

Essentailly we could confirm by TCAD simulations, that the increased leakage of the nPD in 30 µm iEPI was caused by lower doping of the 30 µm iEPI in comparison to the 20 µm iEPI. Figs. 8 and 9 show the extension of the space charge region in dependence on the EPI doping concentration and according leakage current simulations, respectively. The simulation results show the same trend as our measurements. Significant difference in leakage current of photodiodes processed on iEPI of different thickness can be observed only for very lowly doped materials. As depicted in Fig. 10, photodiodes processed on 20 µm and 30 µm iEPI show diverging leakage values only for doping concentrations lower than 1E13/cm³ corrresponding to resistivity values higher than 1 kOhm-cm. Lower leakage of photodiodes in thinner iEPI is caused by the limited extension of the space charge region in depth due to the low resistive substrate placed below the iEPI layer.

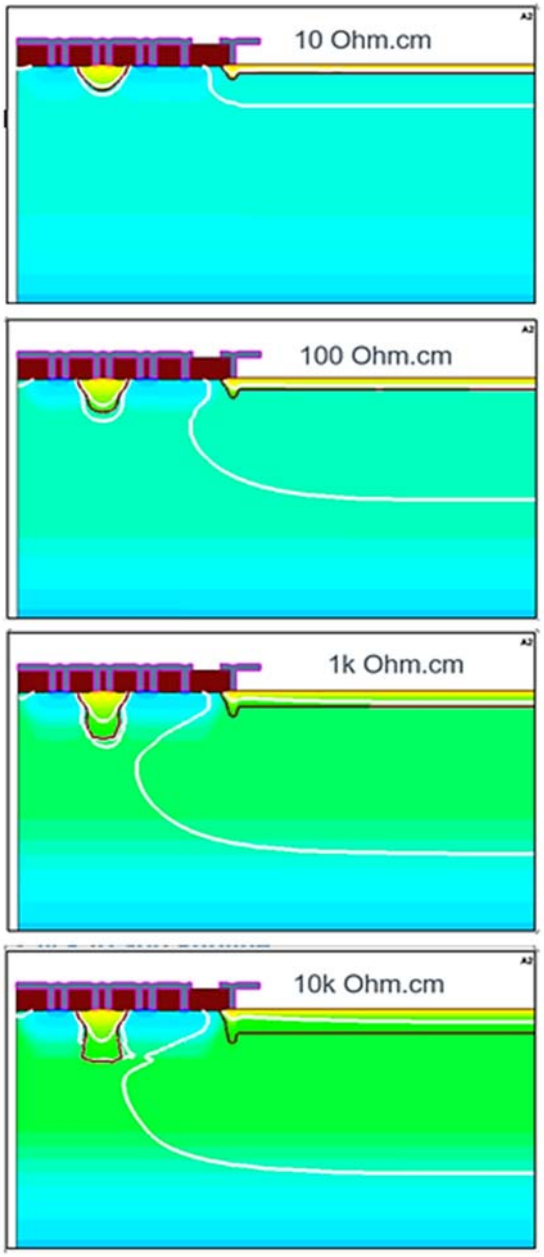

Fig. 8. TCAD simulation of space charge region extension in dependence on EPI doping.

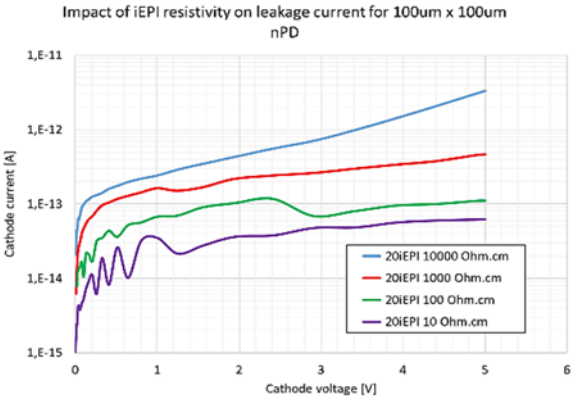

Fig. 9. TCAD simulation of nPD leakae current for different EPI resistivity.

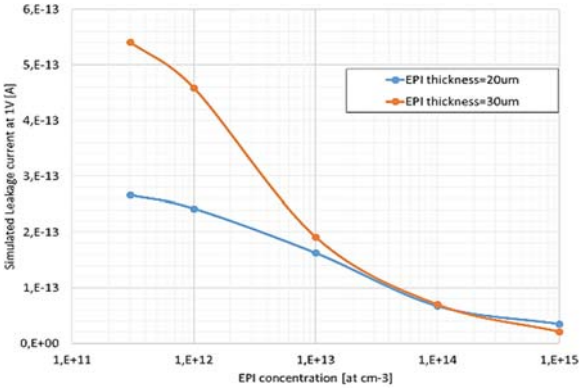

Fig. 10. TCAD simulation of nPD leakae current dependence on iEPI concentration for two EPI thicknesses.

We measured the leakage current of circular nPDs of different size on 20 µm (red curve) and 30 µm iEPI (blue curve) as shown in Fig. 11. Leakage current is linearly dependent on the photodiode diameter.

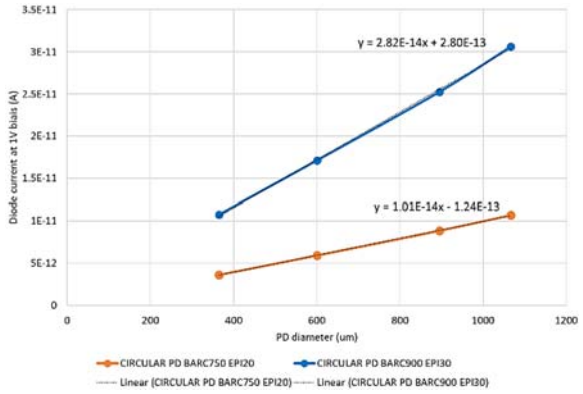

Fig. 11. Measured leakage current magnitude as a function of photodiode diameter.

When designing photodiodes with pnp type guard rings, where the n type contact layer is used for the reduction of photodiode to photodiode electrical and optical crosstalk, care must be taken with respect to photodiode to guard ring spacing. This configuration generates a lateral npn bipolar with the photodiode which increases the leakage current of the photodiode [5-6].

The capacitance of the circular nPD is also dependent on the iEPI thickness and photodiode size. The nPD capacitance is limited by the iEPI thickness because the low resistive substrate placed below the iEPI layer is blocking the extension of the space charge width in depth. Fig. 12 shows that the circular photodiodes' capacitance is linearly dependent on the area of the photodiode while the impact of the BARC is limited.

In addition to circular PIN photodiodes, square PIN photodiodes with a fixed single photodiode geometry of 200 µm × 200 µm are placed. We also processed arrays of 16 square photodiodes (4×4, each 200 µm × 200 µm), 49 square photodiodes (7×7) and 121 square photodiodes (11×11). The cathodes of all the photodiodes placed in an array are connected together. For arrays, the pnp guard ring is only placed around the array while each block has only a p-type substrate contact. Fig. 13 shows the capacitance of a single square photodiode in 20 µm and 30 µm iEPI, as well as the capacitance of different arrays. As observed for circular photodiodes, the capacitance is lowered when the iEPI thickness is increased. Fig. 14 shows the evolution of capacitance of the square PIN photodiode versus the number of photodiodes placed in an array.

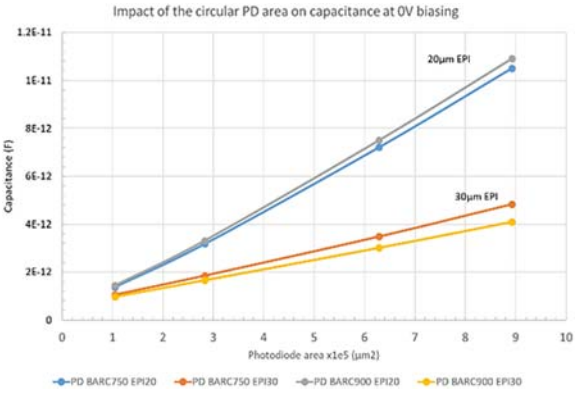

Fig. 12. Evolution of capacitance at 0V with PD area for different iEPI hickness and different BARC thickness.

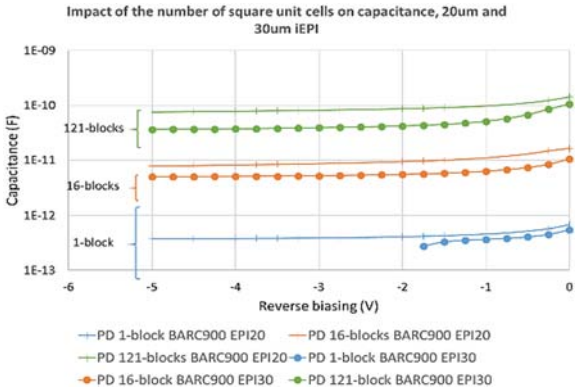

Fig. 13. Impact of scaling of square nPDs in 20 µm and 30 µm iEPI on the capacitance.

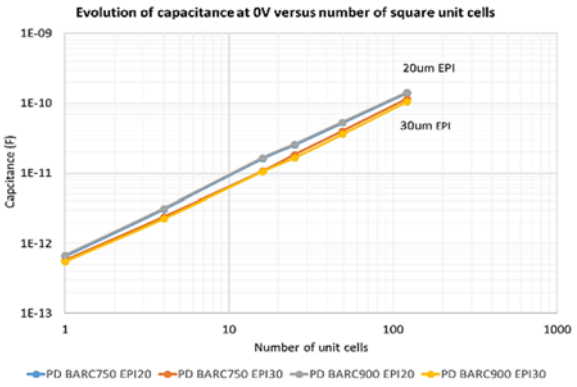

Fig. 14. Evolution of capacitance at 0 V versus number of unit cells for square nPDs.

The capacitance is varying linearly with the number of blocks. As each block has a fixed geometry, the capacitance is varying linearly with the area of the array.

For photodiodes with p-type substrate contact rings instead of pnp guard rings, increasing depth of the p-type substrate contact ring causes decreasing leakage current and increasing capacitance of the photodiodes [3]. The dependence of photodiode leakage and capacitance on the distance between deep p-type substrate contact ring and photodiode is shown in Figs. 15 and 16, respectively. nPDs with 2 µm, 5 µm and 10 µm distance between substrate contact ring and photodiode were analyzed. The base material was 20 µm iEPI. While leakage current shows hardly any dependence on distance, capacitance values vary significantly.

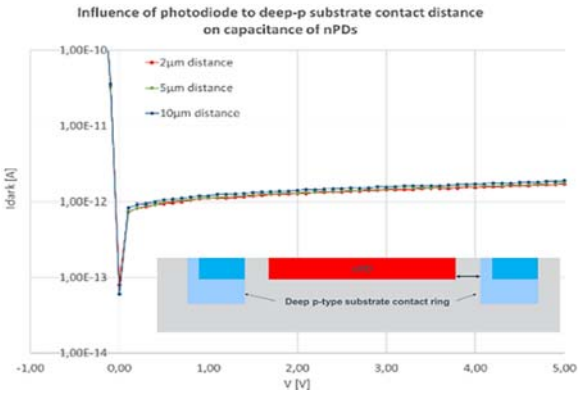

Fig. 15. Impact of nPD distance to deep-p substrate contact on leakage current.

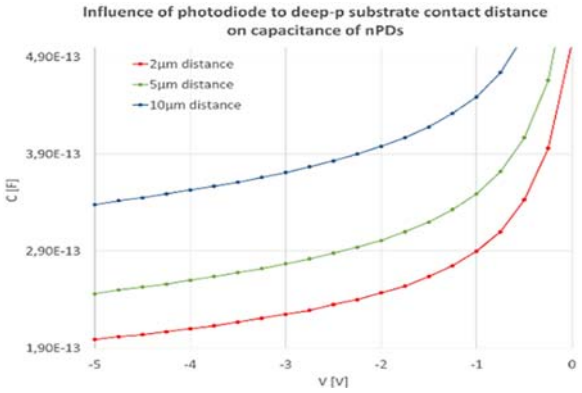

Fig. 16. Impact of nPD distance to deep-p substrate contact on capacitance.

Interdigitated photodiodes (Fig. 1(b)) target for short wavelength light (UV – blue), which is absorbed very close to the Si surface [7]. Therefore UV-blue light is very sensitive to recombination effects due to high doped surface layers. As for our photodiode design the active area between n- and p-fingers is lowly doped, recombination effects are significantly reduced. Electron-hole pairs are created close to the Si surface and the lateral electric field between the fingers collects the generated charge, thus significantly improving the optical response in the respective wavelength range even at 0 V biasing. Fig. 17 shows the influence of finger spacing on spectral responsivity and compares interdigitated photodiodes to nPDs (red curve). For 1.2 µm finger spacing spectral responsivity values as high as 0.21 A/W @ 400 nm and 0.37 A/W @ 500 nm could be achieved.

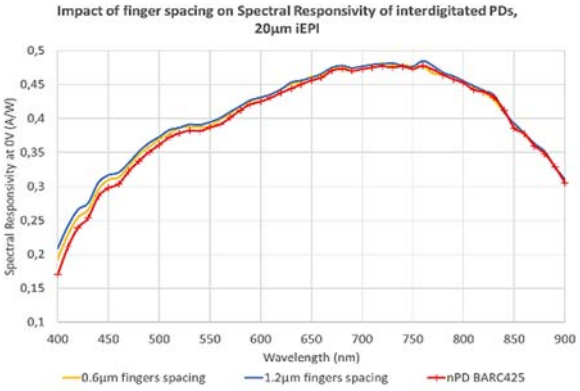

Fig. 17. Influence of finger spacing of interdigitated PDs on spectral responsivity.

Unfortunately, due to the internal npn bipolar action between the n-type and p-type fingers, the leakage current is much stronger with respect to an nPD leakage current as shown in Fig. 18.

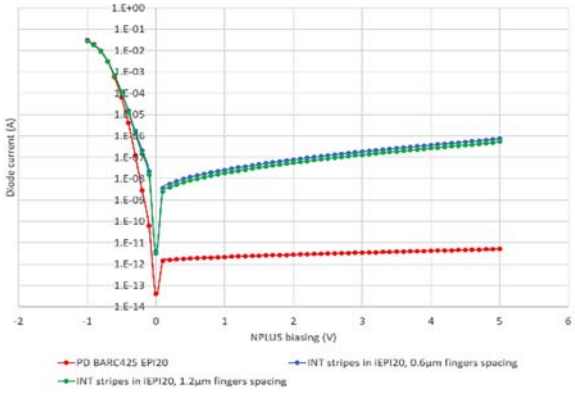

Fig. 18. Leakage current comparison between Interdigitated PDs (blue and green curves) with different n-type/p-type fingers spacing and nPD (red curve).

For the optimized bluePD (Fig. 1(c)), the impact of iEPI thickness on the spectral responsivity is limited due to the fact, that collection photogenerated carriers from UV-blue light happens very close to the Si surface. Fig. 19 shows gray and blue spectral responsivity curves for blue PDs processed on 20 µm and 30 µm thick iEpi material, respectively. There is no difference in spectral responsivity to be seen for the different base materials. The yellow curve represents the spectral responsivity result for a blue PD processed with a BARC layer optimized for λ=425 nm. The

increased spectral response due to the BARC is clearly visible.

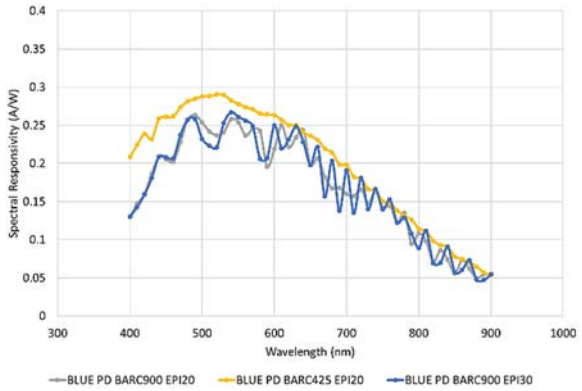

Fig. 19. Spectral responsivity for bluePD as a function of iEPI thickness and BARC optimization.

Because of the internal structure of the bluePD, the leakage current is not dependent on the iEPI thickness, either, and is around 10 pA at a biasing below -1 V for a 150 µm × 150 µm photodiode size designed in a square configuration as can be seen in Fig. 20.

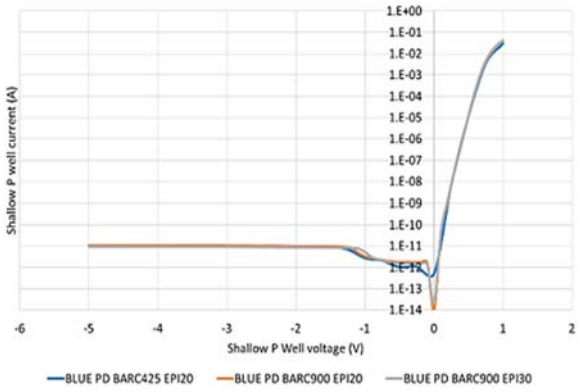

Fig. 20. Leakage Current for bluePD as a function of iEPI thickness and BARC optimization.

Implementation of filter technologies is key for applications such as color sensing, spectral imaging, and ambient light sensing. The required spectral transmission characteristics of the filters is frequently determined by industry standards and customer requests. State of the art and commercially available interference filters deposited on glass or specifically absorbing glasses can be used for such applications. However, for monolithic integrated smart sensors, as described in this paper, the required integration density can't be reached with filters on glass substrates. The filters have to be part of the CMOS fabrication process, taking advantage of the available lithography steps. ams AG offers a large variety of inorganic filters as part of their CMOS fabrication processes, which can be utilized as stand-alone filters together with a photodiode, or in combination as stacked filters.

In order to check the influence of interference filter deposition and patterning on photodiode behaviour, we performed leakage current and spectral responsivity measurements on nPDs with eBARC optimized for 900 nm as well as long pass filters cutting off wavelengths below 850 nm. Fig. 21 shows the spectral responsivity curves for filter devices on 20 µm and 30 µm thick iEPI base material. Fig. 22 shows the leakage current comparison between the filter device described above and the same device processed without filters. Both devices were processed on 20 µm thick iEPI base material. It can be seen that the filter device shows higher leakage, which is most likely caused by the enhanced mechanical stress on the wafers due to filter deposition.

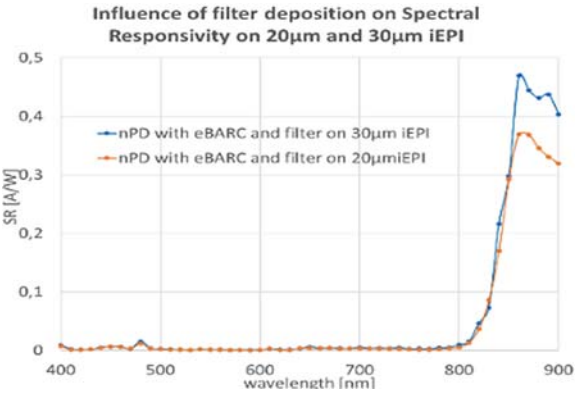

Fig. 21. Influence of long pass filter deposition on spectral responsivity.

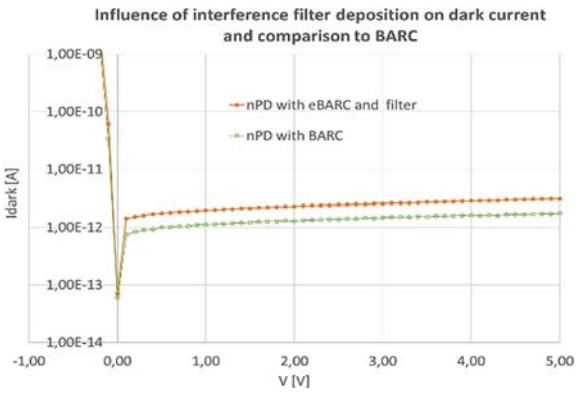

Fig. 22. Influence of long pass filter deposition on leakage current.

4. Conclusions

In this paper, we present the impact of low-doped intrinsic Si Epi material and various backend coatings (BARC, eBARC and filter) on the optical and electrical performance of various PIN photodiodes. Full area PIN photodiodes (high doped n-cathode in p-epitaxial layer) reach a spectral responsivity of 0.63 A/W and 100 % quantum efficiency with the deposition of BARC optimized for λ>750 nm. The leakage current is larger with thicker iEPI thickness and varies from 3.5 pA (20 µm iEPI) to 10 pA (30 µm

iEPI) for photodiodes with 365, diameter at 1V reverse biasing. Their capacitance is reduced for larger iEPI thickness and varies from 0.97 pF (30 µm iEPI) to 1.43 pF (20 µm iEPI) at 0 V biasing. Further tuning of capacitance is possible by distance variations to the surrounding guard rings and substrate contacts. For interdigitated photodiodes, the spectral responsivity in the wavelength range 400 nm to 500 nm can be significantly enhanced compared to full area photodiodes and show values as high as 0.21 A/W @ 400 nm and 0.37 A/W @ 500 nm. Optimized blue photodiodes are not sensible to iEPI thicknesses and have a leakage current of 10 pA for a 150 µm × 150 µm square photodiode.

References

[1]. Simon M. Sze, Kwok K. Ng, Physics of semiconductor devices, 3rd edition, *John Wiley & Sons, Inc.*, Hoboken, NJ, USA, 2007, pp. 671-682.

[2]. I. Jonak-Auer, *et al.*, Monolithic integrated PIN photodiode study with backend stack optimization, in *Proceedings of the 5th International Conference on Sensors Engineering and Electronics Instrumentation Advances (SEIA'19)*, Tenerife (Canary Islands), Spain, 25-27 September 2019, pp. 92-99.

[3]. I. Jonak-Auer, *et al.*, New integration concept of PIN photodiodes in 0.35 µm CMOS technologies, in *Proceedings of the SPIE*, Vol. 8431, 2012.

[4]. I. Jonak-Auer, *et al.*, PIN photodiodes with significantly improved responsivities implemented in a 0.35 µm CMOS/BiCMOS technology, in *Proceedings of the SPIE*, 7719, 77190U, 2010.

[5]. Jordi Teva, *et al.*, Dark current study for CMOS fully integrated-PIN-photodiodes, in *Proceedings of the SPIE - The International Society for Optical Engineering,* Vol. 8073, Optical Sensors 2011; and Photonic Crystal Fibers V; 80731P, 2011.

[6]. Jordi Teva, *et al.*, Gathering effect on Dark Current for CMOS fully integrated-, PIN- photodiodes, in *Proceedings of the SPIE - The International Society for Optical Engineering*, Vol. 7605, 2010.

[7]. H. Zimmermann, *et al.*, Blue-Enhanced PIN Finger Photodiodes in a 0.35-µm SiGe BiCMOS Technology, *IEEE Photonics Technology Letters*, Vol. 21, Issue 22, 2009.

Published by International Frequency Sensor Association (IFSA) Publishing, S. L., 2019 (http://www.sensorsportal.com).

Advances in Microelectronics: Reviews, Vol. 1

Sergey Y. Yurish, Editor

The first volume of '*Advances in Microelectronics: Reviews*' Book Series contains 19 chapters written by 72 authors from academia and industry from 16 countries: Canada, China, Egypt, France, Germany, Iran, Italia, Japan, Malaysia, Norway, Poland, Saudi Arabia, Spain, United Arab Emirates, UK, and USA.

With unique combination of information in each volume, the '*Advances in Microelectronics: Reviews*' Book Series will be of value for scientists and engineers in industry and at universities. In order to offer a fast and easy reading of the state of the art of each topic, every chapter in this book is independent and self-contained. All chapters have the same structure: first an introduction to specific topic under study; second particular field description including sensing applications. Each of chapter is ending by well selected list of references with books, journals, conference proceedings and web sites.

This book ensures that readers will stay at the cutting edge of the field and get the right and effective start point and road map for the further researches and developments.

http://www.sensorsportal.com/HTML/BOOKSTORE/Advances_in_Microelectronics_Vol_1.htm